

# Variations in the Summer Oceanic $p\text{CO}_2$ and Carbon Sink in the Prydz Bay Using the SOM Analysis Approach

Suqing Xu<sup>1</sup>, Keyhong Park<sup>2\*</sup>, Yanmin Wang<sup>3</sup>, Liqi Chen<sup>1\*</sup>, Di Qi<sup>1</sup>, Bingrui Li<sup>4</sup>

1. Key Laboratory of Global Change and Marine-Atmospheric Chemistry, Third Institute of Oceanography, Xiamen 361005, PR China.
2. Division of Polar Ocean Sciences, Korea Polar Research Institute, Incheon 21990, South Korea.
3. Haikou Marine Environment Monitoring Central Station, State Oceanic Administration, Haikou 570100, China.
4. Polar Research Institute of China, Shanghai 200136, China.

Correspondence to: Liqi Chen ([chenliqi@tio.org.cn](mailto:chenliqi@tio.org.cn));

Keyhong Park ([keyhongpark@kopri.re.kr](mailto:keyhongpark@kopri.re.kr))

## Abstract

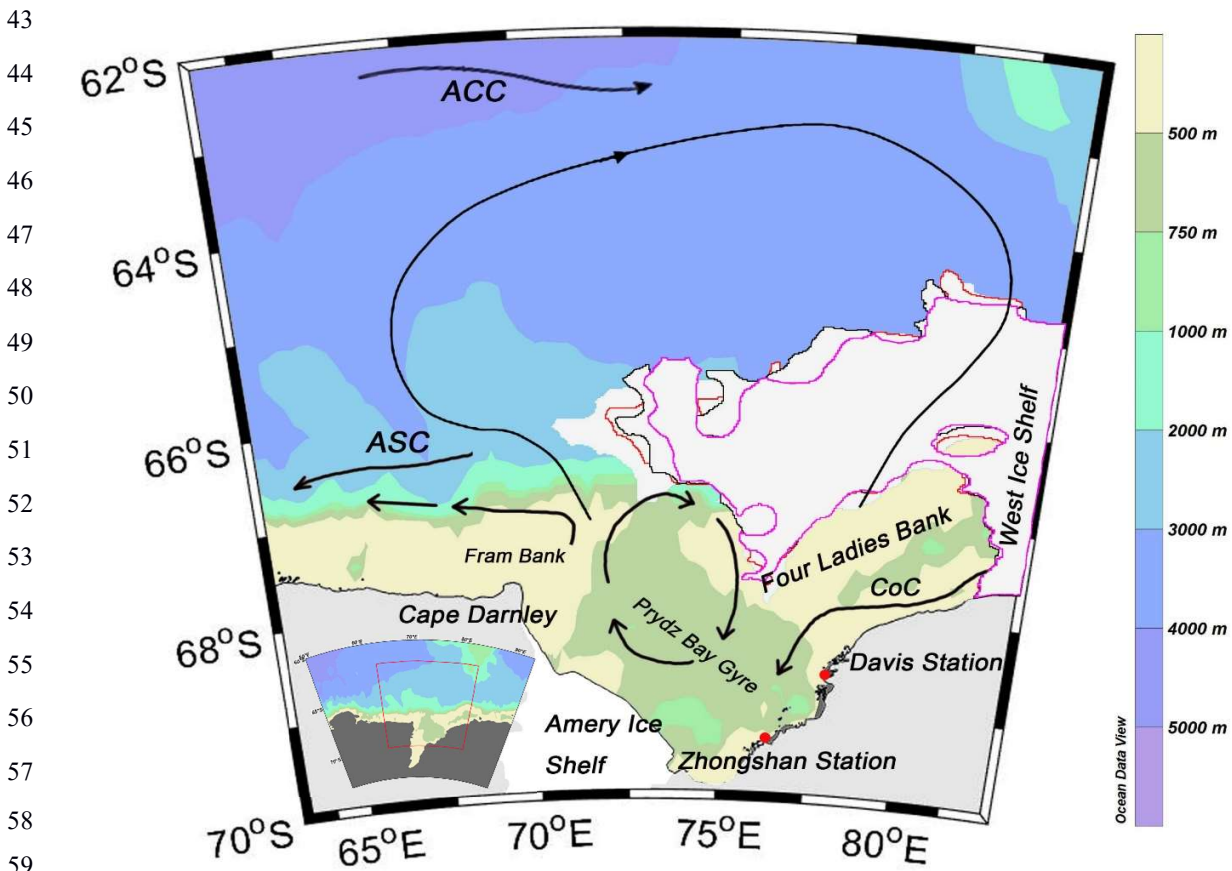
This study applies a neural network technique to produce maps of oceanic surface  $p\text{CO}_2$  in the Prydz Bay in the Southern Ocean on a weekly  $0.1^\circ$  longitude  $\cdot$   $0.1^\circ$  latitude grid based on in situ measurements obtained during the 31<sup>st</sup> CHINARE cruise from February to early March of 2015. This study area was divided into three regions, namely, the Open-ocean region, Sea-ice region and Shelf region. The distribution of oceanic  $p\text{CO}_2$  was mainly affected by physical processes in the Open-ocean region, where mixing and upwelling were the main controls. In the Sea-ice region, oceanic  $p\text{CO}_2$  changed sharply due to the strong change in seasonal ice. In the Shelf region, biological factors were the main control. The weekly oceanic  $p\text{CO}_2$  was estimated using a self-organizing map (SOM) with four proxy parameters (Sea Surface Temperature, Chlorophyll-*a* concentration, Mixed Layer Depth, and Sea Surface Salinity) to overcome the complex relationship between the biogeochemical and physical conditions in the Prydz Bay region. The reconstructed oceanic  $p\text{CO}_2$  data coincide well with the in situ investigated  $p\text{CO}_2$  data from SOCAT, with a root-mean-square error of  $22.14 \mu\text{atm}$ . The Prydz Bay was mainly a strong  $\text{CO}_2$  sink in February 2015, with a monthly averaged uptake of  $23.57 \pm 6.36 \text{ TgC}$ . The oceanic  $\text{CO}_2$  sink is pronounced in the Shelf region due to its lowest oceanic  $p\text{CO}_2$  and peak biological production.

29

### 30 1 Introduction

31 The amount of carbon uptake occurring in the ocean south of 60°S during the transport of  
32 CO<sub>2</sub> to or from the atmosphere is still uncertain despite its importance in regulating atmospheric  
33 carbon and acting as a net sink for anthropogenic carbon (Sweeney et al., 2000, 2002; Morrison  
34 et al., 2001; Sabine et al., 2004; Metzl et al., 2006; Takahashi et al., 2012). This uncertainty  
35 arises from both the strong seasonal and spatial variations that occur around Antarctica and the  
36 difficulty of obtaining field measurements in the region because of its hostile weather and  
37 remoteness.

38 Following the Weddell and Ross seas, the Prydz Bay is the third-largest embayment in the  
39 Antarctic continent. Situated in the Indian Ocean section, the Prydz Bay is located close to the  
40 Amery Ice Shelf to the southwest and the West Ice Shelf to the northeast, with Cape Darnley to  
41 the west and the Zhongshan and Davis stations to the east (Fig. 1). In this region, the water depth  
42 increases sharply northward from 200 m to 3000 m.



60 Fig. 1 Ocean circulations in the Prydz Bay derived from Roden et al. (2013) , Sun et al. (2013), Wu et al.  
61 (2017). ASC: Antarctic Slope Current; CoC: Antarctic Coastal Current; ACC: Antarctic Circumpolar Current.  
62 During the 4-week cruise, the sea ice extent varied as indicated by the contoured white areas: the pink line is  
63 for week-1(20150202-20150209), the black line is for week-2 (20150210-20150217), the red line is for the  
64 week-3 (20150218-20150225) and a fourth contoured area is for week-4 (20150226-20150305).

65 The inner continental shelf is dominated by the Amery Depression, which mostly ranges in  
66 depth from 600 to 700 m. This depression is bordered by two shallow banks (<200 m): the Fram  
67 Bank and the Four Ladies Bank, which form a spatial barrier for water exchange with the outer  
68 oceanic water (Smith and Trégure, 1994). The Antarctic Coastal Current (CoC) flows westward,  
69 bringing in cold waters from the east. When the CoC reaches the shallow Fram Bank, it turns  
70 north and then partly flows westward, while some of it turns eastward, back to the inner shelf,  
71 resulting in the clockwise-rotating Prydz Gyre (see Fig.1). The circulation to the north of the bay  
72 is characterized by a large cyclonic gyre, extending from within the bay to the Antarctic  
73 Divergence at approximately 63°S (Nunes Vaz and Lennon, 1996; Middleton and Humphries,  
74 1989; Smith et al., 1984; Roden et al., 2013; Wu et al., 2017). The inflow of this large gyre hugs  
75 the eastern rim of the bay and favours the onshore intrusions of warmer modified Circumpolar  
76 Deep Water across the continental shelf break (Heil et al., 1996). Westward flow along the shelf,  
77 which is part of the wind-driven Antarctic Slope Current (ASC), supplies water to the Prydz Bay.

78 It has been reported that the Prydz Bay is a strong carbon sink, especially in the austral  
79 summer (Gibson et al., 1999; Gao et al., 2008; Roden et al., 2013). Moreover, studies have  
80 shown that the Prydz Bay region is one of the source regions of Antarctic Bottom Water as well  
81 as the Weddell and Ross seas (Jacobs and Georgi, 1977; Yabukiet al., 2006). It is thus important  
82 to study the carbon cycle in the Prydz Bay. However, the analysis of the temporal variability and  
83 spatial distribution mechanism of oceanic  $p\text{CO}_2$  in the Prydz Bay is limited to cruises or stations  
84 due to its unique physical environment and complicated marine ecosystem (Smith et al., 1984;  
85 Nunes Vaz et al., 1996; Liu et al., 2003). To estimate regional sea-air  $\text{CO}_2$  fluxes, it is necessary  
86 to interpolate between in situ measurements to obtain maps of oceanic  $p\text{CO}_2$ . Such an  
87 interpolation approach, however, is still difficult, as observations are too sparse over both time  
88 and space to capture the high variability in  $p\text{CO}_2$ . Satellites do not measure  $p\text{CO}_2$ , but they do  
89 provide access to the parameters related to the processes that control its variability. The seasonal  
90 and geographical variability of surface water  $p\text{CO}_2$  is indeed much greater than that of  
91 atmospheric  $p\text{CO}_2$ . Therefore, the direction of sea-air  $\text{CO}_2$  transfer is mainly regulated by

92 oceanic  $p\text{CO}_2$ , and the method of spatially and temporarily interpolating in situ measurements of  
93 oceanic  $p\text{CO}_2$  has long been used (Takahashi et al., 2002 and 2009; Olsen et al., 2004; Jamet et  
94 al., 2007; Chierici et al., 2009). In earlier studies, a linear regression extrapolation method was  
95 applied to expand cruise data to study the carbon cycle in the Southern Ocean (Rangama et al.,  
96 2005; Chen et al., 2011; Xu et al., 2016). However, this linear regression relied simply on either  
97 chlorophyll-a (CHL) or sea surface temperature (SST) parameters. Thus, this method can not  
98 sufficiently represent all controlling factors. In this study, we applied self-organizing map (SOM)  
99 analysis to expand our observed data sets and estimate the oceanic  $p\text{CO}_2$  in the Prydz Bay from  
100 February to early March of 2015.

101 The SOM analysis, which is a type of artificial neural network, has been proven to be a  
102 useful method for extracting and classifying features in the geosciences, such as trends in (and  
103 between) input variables (Gibson et al., 2017; Huang et al., 2017b). The SOM uses an  
104 unsupervised learning algorithm (i.e., with no need for a priori, empirical or theoretical  
105 descriptions of input-output relationships), thus enabling us to identify the relationships between  
106 the state variables of the phenomena being analysed, where our understanding of these cannot be  
107 fully described using mathematical equations and thus where applications of knowledge-based  
108 models are limited (Telszewski et al., 2009). In the field of oceanography, SOM has been applied  
109 for the analysis of various properties of seawater, such as sea surface temperature (Iskandar,  
110 2010; Liu et al., 2006), and chlorophyll concentration (Huang et al., 2017a; Silulwane et al.,  
111 2001). In the past decade, SOM has also been applied to produce basin-scale  $p\text{CO}_2$  maps, mainly  
112 in the North Atlantic and Pacific Ocean, by using different proxy parameters (Lafevre et al.,  
113 2005; Friedrich & Oschlies, 2009a, 2009b; Nakaoka et al., 2013; Telszewski et al., 2009; Hales et  
114 al., 2012; Zeng et al., 2015; Laruelle et al., 2017). SOM has been proven to be useful for  
115 expanding the spatial-temporal coverage of direct measurements or for estimating properties  
116 whose satellite observations are technically limited. One of the main benefits of the neural  
117 network method over more traditional techniques is that it provides more accurate  
118 representations of highly variable systems of interconnected water properties (Nakaoka et al.,  
119 2013).

120 We conducted a survey during the 31<sup>st</sup> CHINARE cruise in the Prydz Bay (Fig. 2). This  
121 study aimed to apply the SOM method, combined with remotely sensed data, to reduce the  
122 spatiotemporal scarcity of contemporary  $\Delta p\text{CO}_2$  data and to obtain a better understanding of the

123 capability of carbon absorption in the Prydz Bay from 63°E to 83°E and 64°S to 70°S from  
124 February to early March of 2015.

125 The paper is organized as follows. Section 2 provides descriptions of the in situ  
126 measurements and SOM methods. Section 3 presents the analysis and discussion of the results,  
127 and section 4 presents a summary of this research.

## 128 **2 Data and methods**

### 129 **2.1 In situ data**

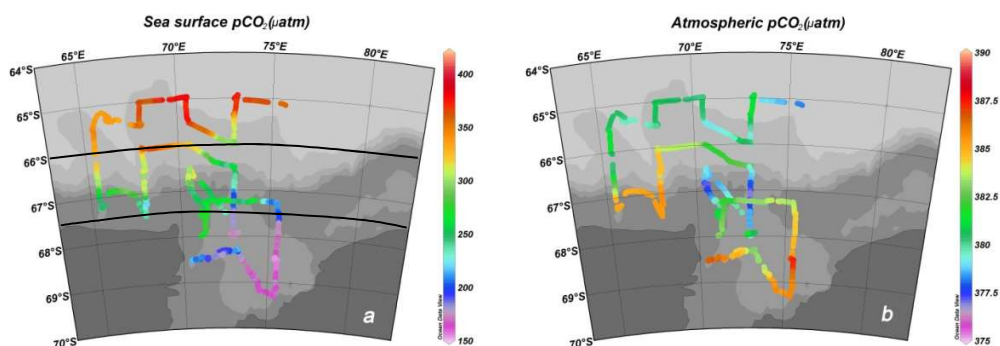
130 The in situ underway  $p\text{CO}_2$  values of marine water and the atmosphere were collected during  
131 the 31<sup>st</sup> CHINARE cruise, when the R/V Xuelong sailed from east to west from the beginning of  
132 February to early March, 2015 (see Fig.2a, b). Sea water at a depth of 5 metres beneath the sea  
133 surface was pumped continuously to the GO system (GO Flowing  $p\text{CO}_2$  system, General  
134 Oceanics Inc., Miami FL, USA), and the partial pressure of the sea surface water was measured  
135 by an infrared analyser (LICOR, USA, Model 7000). The analyser was calibrated every 2.5-3 h  
136 using four standard gases supplied by NOAA's Global Monitoring Division at pressures of 88.82  
137 ppm, 188.36 ppm, 399.47 ppm, and 528.92 ppm. The accuracy of the measured  $p\text{CO}_2$  data is  
138 within 2  $\mu\text{atm}$  (Pierrot et al., 2009). Underway atmospheric  $p\text{CO}_2$  data were simultaneously  
139 collected by the GO system. Due to the biological and physical pumps of carbon cycling in the  
140 ocean (Hardman-Mountford et al., 2009; Bates et al., 1998a, 1998b; Barbini et al., 2003;  
141 Sweeney, 2002), the key factor controlling its gradient in sea-air levels is the solubility of  $\text{CO}_2$ .  
142 The solubility of  $\text{CO}_2$  is affected by temperature and salinity in the water as well as biological  
143 activities, such as phytoplankton taking up  $\text{CO}_2$  through photosynthesis and organisms releasing  
144  $\text{CO}_2$  through respiration (Chen et al., 2011). There are several processes that can influence the  
145 distribution of oceanic  $p\text{CO}_2$ .

146 Sea ice melt has a significant impact on the local stratification and circulation in polar  
147 regions. During freezing, brine is rejected from ice, thereby increasing the sea surface salinity.  
148 When ice begins to melt, fresher water is added into the ocean, thereby diluting the ocean water,  
149 i.e., reducing its salinity. Changes in salinity thus record physical processes. In this study, we  
150 treat salinity as an index for changes in sea ice. The underway SST and conductivity data were  
151 recorded by a Conductivity-Temperature-Depth sensor (CTD, Seabird SBE 21) along the cruise  
152 track. Later, sea surface salinity was calculated based on the recorded conductivity and  
153 temperature data. The distributions of underway SST and SSS are shown in Fig.2c and d.

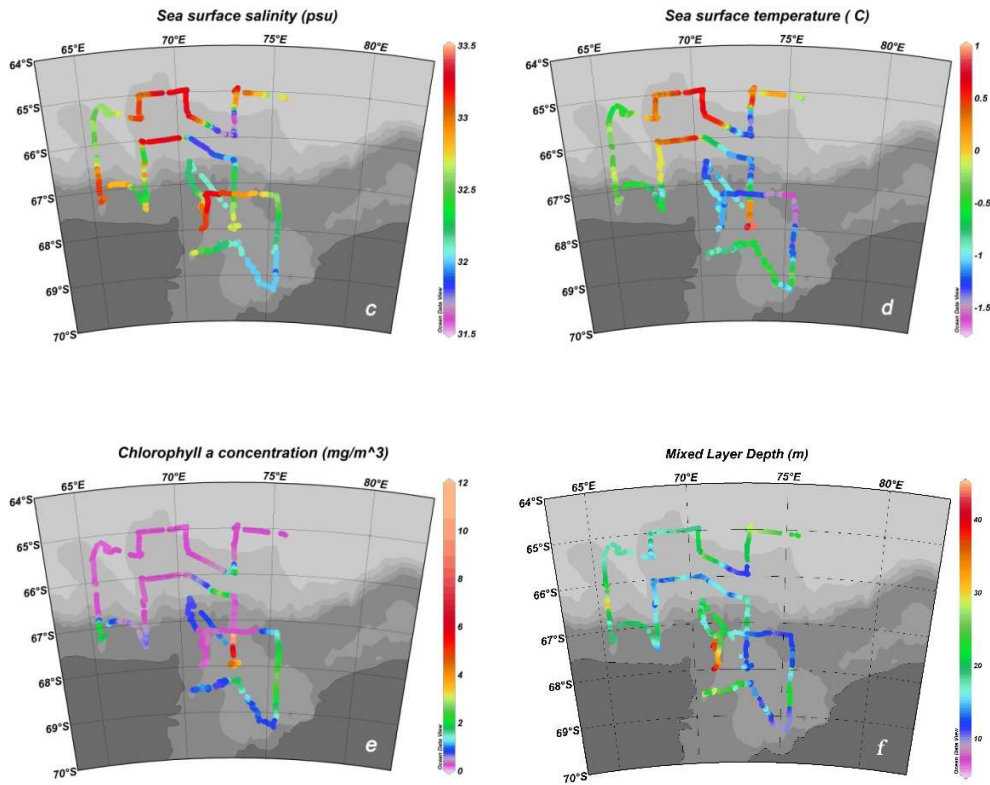
154 In austral summer, when sea ice started to melt, ice algae were released into the seawater,  
155 and the amount of living biological species and primary productivity increased; thus, high  
156 chlorophyll-a values were observed (Liu et al., 2000; Liu et al., 2003). Previous studies have  
157 reported that the summer sink in the Prydz Bay is biologically driven and that the change in  
158  $p\text{CO}_2$  is often well correlated with the surface chlorophyll-a concentration (Rubin et al., 1998;  
159 Gibsonab et al., 1999; Chen et al., 2011; Xu et al., 2016). The chlorophyll-a value is regarded as  
160 an important controlling factor of  $p\text{CO}_2$ . Remote sensing data of chlorophyll-a obtained from  
161 MODIS with a resolution of 4 km (<http://oceancolor.gsfc.nasa.gov>) were interpolated according  
162 to the cruise track (Fig.2e).

163 The ocean mixed layer is characterized as having nearly uniform physical properties  
164 throughout the layer, with a gradient in its properties occurring at the bottom of the layer. The  
165 mixed layer links the atmosphere to the deep ocean. Previous studies have emphasized the  
166 importance of accounting for vertical mixing through the mixed layer depth (MLD, Dandonneau,  
167 1995; Lüger et al., 2004). The stability and stratification of this layer prevent the upward mixing  
168 of nutrients and limit biological production, thus affecting the sea-air  $\text{CO}_2$  exchange. There are  
169 two main methods used to calculate the MLD: one is based on the difference criterion, and one is  
170 based on the gradient criterion. Early studies suggested that the MLD values determined in the  
171 Southern Ocean using the difference criterion are more stable (Brainerd and Gregg, 1995;  
172 Thomson and Fine, 2003). Thus, following Dong et al. (2008), we calculated the mixed layer  
173 depth (see Fig.2f) based on the difference criterion, in which sigma theta changed by  $0.03 \text{ kg/m}^3$ .  
174 The MLD values at the stations along the cruise were later gridded linearly to match the spatial  
175 resolution of the underway measurements.

176



177



178  
179

180

181 Fig.2 The distributions of underway oceanic and atmospheric  $p\text{CO}_2$ , SST, SSS, and CHL gridded from  
182 MODIS, as well as MLD gridded from station surveys, from February to early March.

183

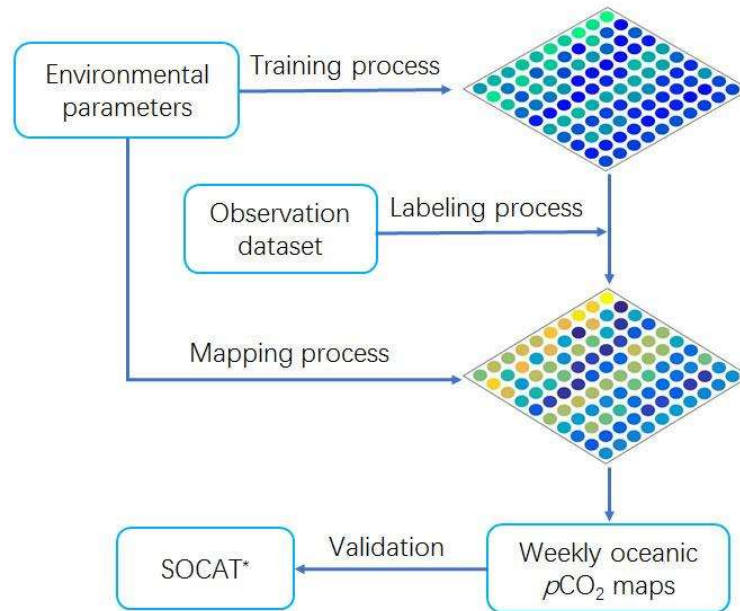
## 184 2.2 SOM method and input variables

185 We hypothesize that oceanic  $p\text{CO}_2$  can be reconstructed using the SOM method with four  
186 proxy parameters (Eq. 1): sea surface temperature (SST), chlorophyll-a concentration (CHL),  
187 mixed layer depth (MLD), and sea surface salinity (SSS).

$$188 \quad p\text{CO}_2^{\text{sca}} = \text{SOM}(\text{SST}, \text{CHL}, \text{MLD}, \text{SSS}) \quad (1)$$

189 The SOM is trained to project the input space of training samples to a feature space  
190 (Kohonen, 1984), which is usually represented by grid points in two-dimensional space. Each  
191 grid point, which is also called a neuron cell, is associated with a weight vector having the same  
192 number of components as the vector of the input data (Zeng et al., 2017). During the SOM  
193 analysis, three steps are taken to estimate the oceanic  $p\text{CO}_2$  fields (see Fig. 3). The input  
194 environmental parameters (in this study, SST, CHL, MLD, and SSS) used to estimate  $p\text{CO}_2$  are  
195 prepared as a vector. Here, the SOM analysis was carried out using the MATLAB SOM tool box  
196 2.0 (Vesanto, 2002). It has been developed by the Laboratory of Computer and Information

197 Science in the Helsinki University of Technology and is available from the following web page:  
198 <http://www.cis.hut.fi/projects/somtoolbox>.



199  
200 Fig. 3. Schematic diagram of the main three steps involved in the SOM neural network calculations used  
201 to obtain weekly  $p\text{CO}_2$  maps for February to early March of 2015.

202 During the training process, each neuron's weight vectors are repeatedly trained by being  
203 presented with the input environmental parameters in the SOM training function. Because SOM  
204 analysis is known to be a powerful technique with which to estimate  $p\text{CO}_2$  based on the non-  
205 linear relationships of the parameters (Telszewski et al., 2009), we assumed that the non-linear  
206 relationships of the proxy parameters are sufficiently represented after the training procedure.  
207 This process results in the clustering of similar neurons and the self-organization of the map. The  
208 observed oceanic  $p\text{CO}_2$  data are not needed in the first step.

209 During the second part of the process, each preconditioned SOM neuron is labelled with an  
210 observation dataset of in situ oceanic  $p\text{CO}_2$  values. The labelling dataset, which consists of the  
211 observed  $p\text{CO}_2$  and normalized SST, CHL, MLD and SSS data, is presented to the neural  
212 network. We used Euclidean distances (i.e., the shortest distances) to select the winner neurons.  
213 After the labelling process, the neurons are represented as five-dimensional vectors.

214 Finally, during the mapping process, the labelled SOM neurons created by the second  
215 process and the trained SOM neurons created by the first process are used to produce the oceanic  
216  $p\text{CO}_2$  value of each winner neuron based on its geographical grid point in the study area.



217 Before the training process, the input training dataset and labelling dataset are analysed and  
 218 prospectively normalized to create an even distribution. The statistics and ranges of the values of  
 219 all variables are presented in Table 1. When the datasets of the four proxy parameters were  
 220 logarithmically normalized, the skewness values of CHL and MLD changed, especially for the  
 221 training dataset. The  $N$  coverage represents the percentage of the training data that are labelled.  
 222 The data  $N$  coverage values of the training data sets of CHL, MLD and SSS are 82.1%, 85% and  
 223 81.1%, respectively, which may be due to their insufficient spatiotemporal coverage and/or bias  
 224 between the labelling and training data sets. The  $N$  coverage of the logarithmic datasets changed  
 225 to 93.6% and to 98.7% for CHL and MLD, respectively. Thus, the common logarithms of the  
 226 CHL and MLD values are used for both the training and labelling datasets to resolve the data  
 227 coverage issue arising from significantly increasing the data coverage as well as to overcome the  
 228 weighting issue arising from the different magnitudes between variables (Ultsch and Röske,  
 229 2002).

230 Table 1. Statistics of labelling and training data sets showing the distribution and coverage of  
 231 each variable.

Coverage of each variable		SST[C]	CHL[mg/m <sup>3</sup> ]	MLD[m]	SSS[psu]
Labelling	Max	0.81	11.13	40.69	33.81
	Min	-1.44	0.17	7.84	32.43
	Mean	-0.27	3.80	14.41	33.27
	Skewness	0.4(-0.2) <sup>#</sup>	0.8(-0.3)	0.9(0.4)	0.6(0.6)
Training	Max	2.48	40.17	48.95	34.17
	Min	-1.8	0.06	10.46	28.64
	Mean	-0.53	1.36	14.79	33.16
	Skewness	0.5(-0.6)	4.3(0.5)	2.6(0.8)	-0.9(-1.0)
	N coverage* (%)	91.3(92.5) <sup>+</sup>	82.1(93.6)	85.0(98.7)	81.1(80.4)

232 # The skewness of the common logarithm of each variable is shown in parentheses.

233 \* [number of training data within the labelling data range]/[total number of training data]

234 + The percent labelling data coverage of normalized variables is shown in parentheses

235 In this study, we construct weekly oceanic  $p\text{CO}_2$  maps from February to early March of  
 236 2015 using four datasets, i.e., SST, CHL, MLD, and SSS. Considering the size of our study  
 237 region, we chose a spatial resolution of  $0.1^\circ$  latitude by  $0.1^\circ$  longitude. For SST, we used daily  
 238 data from AVHRR ONLY (<https://www.ncdc.noaa.gov/oisst>) with a  $1/4^\circ$  spatial resolution (see  
 239 Fig.S1). CHL data represent the 8-D composite chlorophyll-a data from MODIS-Aqua

240 (<http://oceancolor.gsfc.nasa.gov>) with a spatial resolution of 4 km (see Fig.S2). We also used the  
241 daily SSS and MLD data (see Fig.S3-4) from the 1/12° global analysis and forecast product from  
242 the Copernicus Marine Environment Monitoring Service (CMEMS,  
243 <http://marine.copernicus.eu/>). Sea ice concentration data are from the daily 3.125-km AMSR2  
244 dataset (Sprien et al., 2008, available on <https://seaice.uni-bremen.de>, see Fig.S5).

245 All daily datasets were first averaged to 8-day fields, which are regarded as weekly in this  
246 study. The period from the beginning of February to early March comprises four independent  
247 week series: week-1 (from 02/02/2015 to 02/09/2015), week-2 (from 02/10/2015 to 02/17/2015),  
248 week-3 (from 02/18/2015 to 02/25/2015), and week-4 (from 02/26/2015 to 03/05/2015). The  
249 weekly proxy parameters (SCMS) were further re-gridded to a horizontal resolution of 0.1°·0.1°  
250 using the Kriging method. In the SOM analyses, input vectors with missing elements are  
251 excluded. We compared the assimilated datasets of SST from AVHRR with the in situ  
252 measurements obtained by CTD along the cruise. Their correlation is 0.97, and their root-mean-  
253 square error (RMSE) is 0.2°C. Comparing the SSS and MLD fields from the Global Forecast  
254 system with the in situ measurements yields correlations of 0.76 and 0.74 and RMSEs of 0.41  
255 psu and 5.15 m, respectively. The uncertainty of the MODIS CHL data in the Southern Ocean is  
256 approximately 35% (Xu et al., 2016). For the labelling procedure, the observed oceanic  $p\text{CO}_2$   
257 together with the corresponding in situ SST, SSS, MLD, and MODIS CHL products in vector  
258 form are used as the input dataset.

### 259 **2.3 Validation of SOM-derived oceanic $p\text{CO}_2$**

260 More realistic  $p\text{CO}_2$  estimates are expected from SOM analyses when the distribution and  
261 variation ranges of the labelling variables closely reflect those of the training data sets (Nakaoka  
262 et al., 2013). However, our underway measurements of  $p\text{CO}_2$  values have spatiotemporal  
263 limitations preventing them from covering the range of variation of the training data sets. To  
264 validate the oceanic  $p\text{CO}_2$  values reconstructed by the SOM analysis, we used the fugacity of  
265 oceanic  $\text{CO}_2$  datasets from the Surface Ocean  $\text{CO}_2$  Atlas (hereafter referred to as “SOCAT”  
266 data, <http://www.socat.info>) version 5 database (Bakker et al., 2016). We selected the dataset from  
267 SOCAT (the EXPCODE is 09AR20150128, see cruise in Fig. 4a) that coincided with the same  
268 period as our study. The cruise lasted from Feb. 6 to Feb. 27, 2015, and  $f\text{CO}_2$  measurements were  
269 made every 1 min at a resolution of 0.01°. We recalculated  $p\text{CO}_2$  values based on the obtained  
270  $f\text{CO}_2$  values provided by the SOCAT data using the fugacity correction (Pfeil et al., 2013).

271

## 272 **2.4 Carbon uptake in the Prydz Bay**

273 The flux of CO<sub>2</sub> between the atmosphere and the ocean was determined using  $\Delta p\text{CO}_2$  and  
274 the transfer velocity across the sea-air interface, as shown in Eq. 2, where K is the gas transfer  
275 velocity (in cm h<sup>-1</sup>), and the quadratic relationship between wind speed (in units of m s<sup>-1</sup>) and the  
276 Schmidt number is expressed as  $(\text{Sc}/660)^{-0.5}$ . L is the solubility of CO<sub>2</sub> in seawater (in mol litre<sup>-1</sup>  
277 atm<sup>-1</sup>) (Weiss, 1974). For the weekly estimation in this study, the scaling factor for the gas  
278 transfer rate is changed to 0.251 for shorter time scales and intermediate wind speed ranges  
279 (Wanninkhof, 2014). Considering the unit conversion factor (Takahashi et al., 2009), the weekly  
280 sea-air carbon flux in the Prydz Bay can be estimated using Eq. (3):

$$281 \quad Flux_{\text{sea-air}} = K \times L \times \Delta p\text{CO}_2 \quad (2)$$

$$282 \quad Flux_{\text{sea-air}} [\text{g C}/(\text{m}^2 \cdot \text{week})] = 30.8 \times 10^{-4} \times U^2 \times (p\text{CO}_2^{\text{sea}} - p\text{CO}_2^{\text{air}}) \quad (3)$$

283 where U represents the wind speed 10 m above sea level, and  $p\text{CO}_2^{\text{sea}}$  and  $p\text{CO}_2^{\text{air}}$  are the partial  
284 pressures of CO<sub>2</sub> in sea water and the atmosphere, respectively.

285 We downloaded weekly ASCAT wind speed data (<http://www.remss.com/>, see Fig. S6)  
286 with a resolution of 1/4° and then gridded the dataset to fit the 0.1° longitude · 0.1° latitude  
287 spatial resolution of the SOM-derived oceanic  $p\text{CO}_2$ . We gridded the atmospheric  $p\text{CO}_2$  data  
288 collected along the cruise track to fit the spatial resolution of the SOM-derived oceanic  $p\text{CO}_2$   
289 data using a linear method. The total carbon uptake was then obtained by accumulating the flux  
290 of each grid in each area according to Jiang et al. (2008) and using the proportion of ice-free  
291 areas (Takahashi et al., 2012). When the ice concentration is less than 10% in a grid, we regard  
292 the grid box as comprising all water. When the ice concentration falls between 10% and 90%, the  
293 flux is computed as being proportional to the water area. In the cases of leads or polynyas due to  
294 the dynamic motion of sea ice (Worby et al., 2008), we assume the grid box to be 10% open  
295 water when the satellite sea ice cover is greater than 90%.

## 296 **3 Results and discussion**

### 297 **3.1 The distributions of underway measurements**

298 During austral summer, daylight lasts longer and solar radiation increases. With increasing  
299 sea surface temperature, ice shelves break and sea ice melts, resulting in the stratification of the  
300 water column. Starting in the beginning of February, the R/V Xuelong sailed from east to west  
301 along the sea ice edge, and its underway measurements are shown in Fig.2. Based on the water

302 depth and especially the different ranges of oceanic  $p\text{CO}_2$  (see Fig.2a and Table2), the study area  
303 can be roughly divided into three regions, namely, the Open-ocean region, Sea-ice region and  
304 Shelf region (see Table2).

305 The Open-ocean region ranges northward from  $66^\circ\text{S}$  to  $64^\circ\text{S}$ , where the Antarctic  
306 Divergence Zone is located and water depths are greater than 3000 m. In the Open-ocean region,  
307 the oceanic  $p\text{CO}_2$  was the highest, varying from  $291.98 \mu\text{atm}$  to  $379.31 \mu\text{atm}$ , with a regional  
308 mean value of  $341.48 \mu\text{atm}$ . The Antarctic Divergence Zone was characterized by high nutrient  
309 concentrations and low chlorophyll concentrations, with high  $p\text{CO}_2$  attributed to the upwelling of  
310 deep waters, thus suggesting the importance of physical processes in this area (Burkill et al.,  
311 1995; Edwards et al., 2004). The underway sea surface temperatures in this region are relatively  
312 high, with an average value of  $-0.23^\circ\text{C}$  due to the upwelling of Circumpolar Deep Water (CDW),  
313 while at the sea ice edge ( $73^\circ\text{E}$ ,  $65.5^\circ\text{S}$  to  $72^\circ\text{E}$ ,  $65.8^\circ\text{S}$ ), the SST decreased to less than  $-1^\circ\text{C}$ .  
314 From  $67.5^\circ\text{E}$  westward, affected by the large gyre, cold water from high latitudes lowered the  
315 SST to less than  $0^\circ\text{C}$ . Near the sea ice edge, SSS decreased quickly to 31.7 psu due to the diluted  
316 water; along the  $65^\circ\text{S}$  cruise, it reached 33.3 psu; then, moving westward from  $67.5^\circ\text{E}$ , affected  
317 by the fresher and colder water brought by the large gyre, it decreased to 32.5 psu. The satellite  
318 chlorophyll-a image showed that the regional mean was as low as  $0.45 \text{ mg/m}^3$ , except when the  
319 vessel near the sea ice edge recorded CHL values that increased to  $2.26 \text{ mg/m}^3$ . The lowest  
320  $p\text{CO}_2$  value was found near the sea ice edge due to biological uptake. The distribution of MLD  
321 varied along the cruise. Near the sea ice edge, because of the melting of ice and direct solar  
322 warming, a low-density cap existed over the water column, and the MLD was as shallow as  
323 10.21 m. The maximum value of MLD in the Open-ocean region was 31.67 m. In the Open-  
324 ocean region, atmospheric  $p\text{CO}_2$  varied from  $374.6 \mu\text{atm}$  to  $387.8 \mu\text{atm}$ . Along the  $65^\circ\text{E}$  cruise in  
325 the eastern part of the Open-ocean region, the oceanic  $p\text{CO}_2$  was relatively high, reaching  
326 equilibrium with atmospheric  $p\text{CO}_2$ . In the western part of this region, the oceanic  $p\text{CO}_2$   
327 decreased slightly due to the mixture of low  $p\text{CO}_2$  from higher latitudes brought by the large  
328 gyre. Mixing and upwelling were the dominant factors affecting the oceanic  $p\text{CO}_2$  in this region.

329 The seasonal Sea-ice region (from  $66^\circ\text{S}$  to  $67.25^\circ\text{S}$ ) is located between the Open-ocean  
330 region and the Shelf region. In this sector, sea ice changed strongly, and the water depth varied  
331 sharply from 700 m to 2000 m. The oceanic  $p\text{CO}_2$  values ranged from  $190.46 \mu\text{atm}$  to  $364.43$   
332  $\mu\text{atm}$ , with a regional mean value of  $276.48 \mu\text{atm}$ . Sea ice continued to change and reform from

333 late February to the beginning of March (Fig. 6). The regional mean sea surface temperature  
 334 decreased slightly compared to that in the Open-ocean region, and the average value was -  
 335 0.72°C. With the rapid changes in sea ice, the sea surface temperature and salinity varied sharply  
 336 from -1.3°C to 0.5°C and from 31.8 psu to 33.3 psu, respectively. When sea ice melted, the water  
 337 temperature increased, biological activity increased, and the chlorophyll-a value increased  
 338 slightly to reach a regional average of 0.59 mg/m<sup>3</sup>. Due to the rapid change in sea ice cover, the  
 339 value of MLD varied from 12.8 m to 30.9 m.

340 The Shelf region (from 67.25°S southward) is characterized by shallow depths of less than  
 341 700 m, and it is surrounded by the Amery Ice Shelf and the West Ice Shelf. Water inside the  
 342 Shelf region is formed by the modification of low-temperature and high-salinity shelf water  
 343 (Smith et al., 1984). The Prydz Bay coastal current flows from east to west in the semi-closed  
 344 bay. The oceanic *p*CO<sub>2</sub> values in this region were the lowest of those in all three sectors; these  
 345 values ranged from 151.70 μatm to 277.78 μatm, with a regional average of 198.72 μatm. A  
 346 fresher, warmer surface layer is always present over the bay, which is known as the Antarctic  
 347 Surface Water (ASW). During our study period, the Shelf region was the least ice-covered  
 348 region. A large volume of freshwater was released into the bay, resulting in low sea surface  
 349 temperature (an average of -0.61°C) and salinity (an average of 32.4 psu) values. As shown in  
 350 Fig.2f, the mixed layer depth in most of the inner shelf is low. Due to the vast shrinking of sea  
 351 ice and strong stratification in the upper water, algal blooming occurred and chlorophyll values  
 352 were high, with an average of 1.93 mg/m<sup>3</sup>. The chlorophyll-a value was remarkably high,  
 353 reaching 11.04 mg/m<sup>3</sup> when sea ice retreated eastwardly from 72.3°E, 67.3°S to 72.7°E, 68°S.  
 354 The biological pump became the dominant factor controlling the distribution of oceanic *p*CO<sub>2</sub>. In  
 355 the bay mouth close to the Fram Bank, due to local upwelling, the water salinity increased  
 356 remarkably to approximately 33.2 psu.

357 Table 2 The regional mean values of underway measurements in three sub-regions

	<i>p</i> CO <sub>2</sub> [μatm]	SST [° ]	CHL [mg/m <sup>3</sup> ]	MLD [m]	SSS [psu]
Open-ocean region (66°S - 64°S)	341.48	-0.23	0.45	20.13	32.61
Sea-ice region (66°S - 67.25°S)	276.48	-0.72	0.59	19.44	32.42
Shelf region (67.25°S - 70°S)	198.72	-0.61	1.95	16.84	32.46

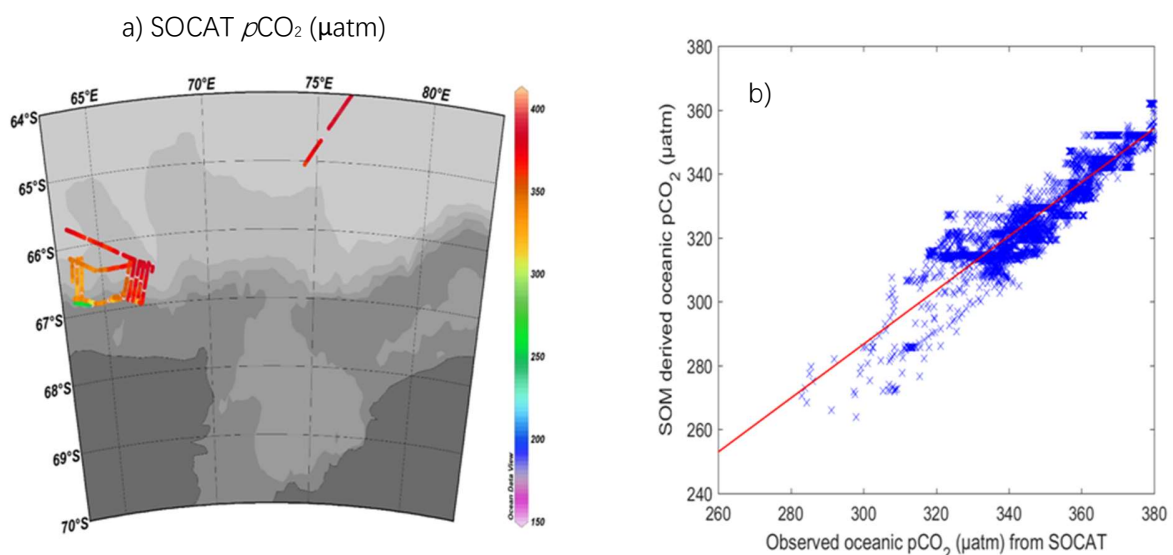
358

359 **3.2 Quality and maps of SOM-derived oceanic  $p\text{CO}_2$**

360 We selected SOM-derived oceanic  $p\text{CO}_2$  values to fit the cruise track of SOCAT for the  
 361 same period in February 2015 using a nearest-grid method. The RMSE between the SOCAT data  
 362 and the SOM-derived result was calculated as follows:

$$363 \quad RMSE = \sqrt{\frac{\sum(p\text{CO}_2^{sea}(SOM) - p\text{CO}_2^{sea}(SOC))^2}{n}} \quad (4)$$

364 where  $n$  is the number of validation datasets. The RMSE can be interpreted as an estimation of  
 365 the uncertainty in the SOM-derived oceanic  $p\text{CO}_2$  in the Prydz Bay. In this study, the RMSE of  
 366 the SOM-derived oceanic  $p\text{CO}_2$  and SOCAT datasets is 22.14  $\mu\text{atm}$ , and the correlation  
 367 coefficient  $R^2$  is 0.82. The absolute mean difference is 23.58  $\mu\text{atm}$ . The RMSE obtained in our  
 368 study is consistent with the accuracies (6.9  $\mu\text{atm}$  to 24.9  $\mu\text{atm}$ ) obtained in previous studies that  
 369 used neuron methods to reconstruct oceanic  $p\text{CO}_2$  (Nakaoka et al., 2013; Zeng et al., 2002;  
 370 Sarma et al., 2006; Jo Y H et al., 2012; Hales et al., 2012; Telszewski et al., 2009). The precision  
 371 of this study is on the high side of those that have been previously reported. The slope of the  
 372 scatter plot indicates that the SOM-derived oceanic  $p\text{CO}_2$  data are lower than the SOCAT data  
 373 (see Fig. 4b). Thus, the precision of these data may have greater uncertainty because the SOCAT  
 374 dataset does not cover the low- $p\text{CO}_2$  area towards the south. Thus, increasing the spatial  
 375 coverage of the labelling data will help increase the precision of the SOM-derived oceanic  $p\text{CO}_2$ .



376 Fig. 4 a) The cruise lines from SOCAT used to validate the SOM-derived oceanic  $p\text{CO}_2$  for the study period in  
 377 2015; b) comparison between the SOM-derived and observed SOCAT oceanic  $p\text{CO}_2$  data.

378

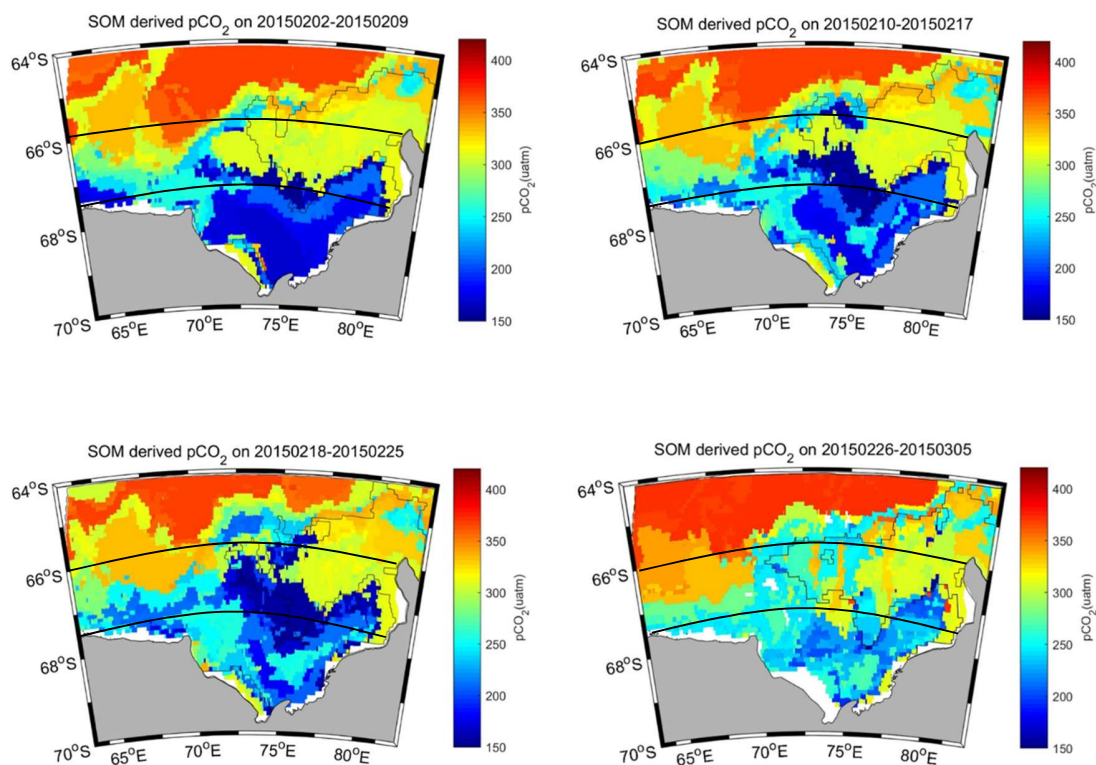
### 379 **3.3 Spatial and temporal distributions of SOM-derived oceanic $p\text{CO}_2$**

380 The weekly mean maps of SOM-derived oceanic  $p\text{CO}_2$  in the Prydz Bay are shown in Fig. 5.  
381 In the Open-ocean region, the oceanic  $p\text{CO}_2$  values were higher than those in the other two  
382 regions due to the upwelling of the CDW. During all four weeks, this region was nearly ice-free,  
383 while the average sea ice coverage was 18.14% due to the presence of permanent sea ice (see  
384 Fig.6). The oceanic  $p\text{CO}_2$  distribution decreased from east to west in the Open-ocean region, with  
385 lower values observed at the edge of sea ice. In the western part of the Open-ocean region,  
386 oceanic  $p\text{CO}_2$  decreased due to mixing with low oceanic  $p\text{CO}_2$  flowing from high-latitude  
387 regions caused by the large gyre. From week-1 to week-4, the maximum oceanic  $p\text{CO}_2$  increased  
388 slightly and reached 381.42  $\mu\text{atm}$ , which was equivalent to the  $p\text{CO}_2$  value of the atmosphere.

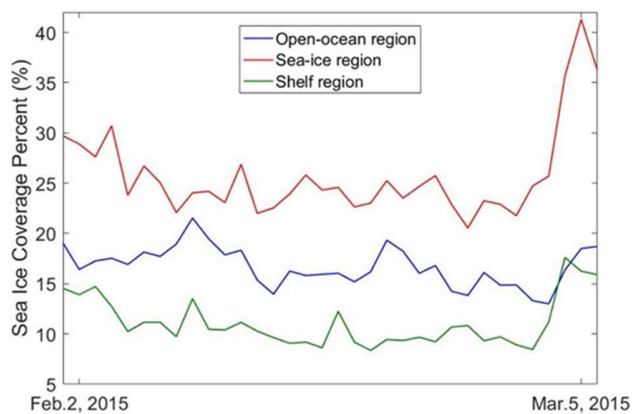
389 In the Sea-ice region, sea ice continued to rapidly melt and reform. The weekly mean sea ice  
390 coverage percentage was 29.54%, occupying nearly one-third of the Sea-ice region. As shown in  
391 Fig.5, the gradient of the oceanic  $p\text{CO}_2$  distribution increased from south to north affected by the  
392 flow coming from the Shelf region by the large gyre. In the eastern part of this region, adjacent  
393 to the sea ice edge, the oceanic  $p\text{CO}_2$  values were lower. The oceanic  $p\text{CO}_2$  changed sharply from  
394 155.86  $\mu\text{atm}$  (near the sea ice edge) to 365.11  $\mu\text{atm}$  (close to the Open-ocean region).

395 In austral winter, the entire Prydz Bay basin is fully covered by sea ice, except in a few  
396 areas, i.e., the polynyas, which remain open due to katabatic winds (Liu et al., 2017). When the  
397 austral summer starts, due to coincident high wind speeds, monthly peak tides, and/or the effect  
398 of penetrating ocean swells, the sea ice in the Shelf region starts to melt first in early summer  
399 (Lei et al., 2010), forming the Prydz Bay Polynya. The semi-closed polynya functions as a  
400 barrier for water exchange in the Shelf region and causes a lack of significant bottom water  
401 production, hindering the outflow of continental shelf water and the inflow of Antarctic circle  
402 deep water, resulting in the longer residence time of vast melting water and enhanced  
403 stratification (Sun et al., 2013). Due to vast melting of the sea ice, the sea surface salinity  
404 decreased and algae bloomed; biological productivity promptly increased, and the chlorophyll-a  
405 concentration reached its peak value. As shown in Fig. 5, the distribution of oceanic  $p\text{CO}_2$  in the  
406 Shelf region was characterized by its lowest values. The obvious drawdown of oceanic  
407  $p\text{CO}_2$  occurred in the Shelf region due to phytoplankton photosynthesis during this summer  
408 bloom. The lowest oceanic  $p\text{CO}_2$  in the Shelf region was 153.83  $\mu\text{atm}$ , except at the edge of the

409 West Ice Shelf, where the Shelf oceanic  $p\text{CO}_2$  exceeded 300  $\mu\text{atm}$ . The oceanic  $p\text{CO}_2$  was the  
 410 lowest in week-1, which coincided with a peak in chlorophyll-a, as evidenced by satellite  
 411 images. The regional oceanic  $p\text{CO}_2$  increased slightly in week-4 compared to the other three  
 412 weeks.



413  
 414 Fig.5 Distribution of weekly mean SOM-derived oceanic  $p\text{CO}_2$  in the Prydz Bay (unit:  $\mu\text{atm}$ ) from Feb.  
 415 2, 2015 to Mar. 5, 2015. The black contour represents a sea ice concentration of 15%.



416



417 Fig. 6 Percentage of sea ice coverage in three sub-regions from Feb. 2, 2015 to Mar. 5, 2015 (blue: Open-  
 418 ocean region; red: Sea-ice region; green: Shelf region).

### 419 3.4 Carbon uptake in the Prydz Bay

420 During our study period, the entire region was undersaturated, with CO<sub>2</sub> being absorbed  
 421 by the ocean. The regional averaged ocean-air pCO<sub>2</sub> difference ( $\Delta p\text{CO}_2$ ) was highest in the Shelf  
 422 region, followed by the Sea-ice region and Open-ocean region (see Table3). The regional and  
 423 weekly mean  $\Delta p\text{CO}_2$  in the Shelf region changed from -184.31  $\mu\text{atm}$  in week-1 to -141.00  $\mu\text{atm}$   
 424 in week-2 as chlorophyll decreased. The  $\Delta p\text{CO}_2$  in the Sea-ice region and Open-ocean region  
 425 showed the same patterns, increasing from week-1 to week-3 and then decreasing in week-4.  
 426 Based on the  $\Delta p\text{CO}_2$  and wind speed data, the uptake of CO<sub>2</sub> in these three regions is presented  
 427 in Table3. The uncertainty of the carbon uptake depends on the errors associated with the wind  
 428 speed, the scaling factor and the accuracy of the SOM-derived pCO<sub>2</sub> according to Eq.3. The  
 429 scaling factor will yield a 20% uncertainty in the regional flux estimation. The errors in the wind  
 430 speeds of the ASCAT dataset are assumed to be 6% (Xu et al., 2016); the error in the quadratic  
 431 wind speed is 12%. The RMSE of the SOM-derived pCO<sub>2</sub> is 22.14  $\mu\text{atm}$ . Considering the errors  
 432 described above and the uncertainty occurring when the sea-air computation expression is  
 433 simplified (1.39%, Xu et al., 2016), the total uncertainty of the final uptake is 27%. In the Shelf  
 434 region, the low oceanic pCO<sub>2</sub> levels drove relatively intensive CO<sub>2</sub> uptake from the atmosphere.  
 435 The carbon uptake in the Shelf region changed mildly from week-1 ( $2.51 \pm 0.68 \text{ TgC}$ ,  $10^{12}$   
 436 gram=Tg) to week-2 ( $2.77 \pm 0.75 \text{ TgC}$ ). In contrast, in week-3, the wind speed slowed down,  
 437 resulting in the uptake of CO<sub>2</sub> in the Shelf region decreasing to  $2.10 \pm 0.57 \text{ TgC}$ . In week-4, even  
 438 though the  $\Delta p\text{CO}_2$  was the lowest of all four weeks, the total absorption still increased to  
 439  $2.63 \pm 0.715 \text{ TgC}$  due to the high wind speed (with an average value of 7.92 m/s). The total  
 440 carbon uptake in the three regions of the Prydz Bay, integrated from February to early March  
 441 of 2015, was  $23.57 \text{ TgC}$ , with an uncertainty of  $\pm 6.36 \text{ TgC}$ .

442 Table3 Regional and weekly mean  $\Delta p\text{CO}_2$ , wind speed and uptake of CO<sub>2</sub> in three sub-  
 443 regions (negative values represent directions moving from air to sea).

		Week-1	Week-2	Week-3	Week-4	Uptake in 4 weeks [Tg]
Open-ocean region (66°S - 64°S)	$\Delta p\text{CO}_2$ [ $\mu\text{atm}$ ]	-34.11	-42.69	-51.94	-34.08	
	Wind speed [m/s]	7.82	8.54	7.02	9.31	-5.74
	Uptake [Tg]	-1.08	-1.55	-1.51	-1.60	
Sea-ice region (66°S - 67.25°S)	$\Delta p\text{CO}_2$ [ $\mu\text{atm}$ ]	-115.92	-119.83	-127.74	-86.72	
	Wind speed [m/s]	7.67	8.17	6.39	8.36	-7.82

	Uptake [Tg]	-2.11	-2.35	-1.73	-1.63	
Shelf region	$\Delta p\text{CO}_2$ [ $\mu\text{atm}$ ]	-184.32	-170.23	-158.61	-141.03	
(67.25°S - 70°S)	Wind speed [m/s]	6.92	7.27	6.67	7.92	-10.01
	Uptake [Tg]	-2.51	-2.77	-2.10	-2.63	

444

445 Roden et al. (2013) estimated the coastal Prydz Bay to be an annual net sink for CO<sub>2</sub> of  
446 0.54±0.11 mol/(m<sup>2</sup>·year), i.e., 1.48±0.3 g/(m<sup>2</sup>·week). Gibsonab et al. (1999) estimated the  
447 average sea-air flux in the summer ice-free period to be more than 30 mmol/(m<sup>2</sup>·day), i.e., 9.2  
448 g/(m<sup>2</sup>·week). Our study suggests that the sea-air flux during the strongest period of the year, i.e.,  
449 February, could be much larger. The average flux obtained here, 18.84 g/(m<sup>2</sup>·week), is twice as  
450 large as the average value estimated over a longer period (November to February) reported by  
451 Gibsonab et al. (1999).

452 As the region recording the strongest surface unsaturation of these three regions in summer,  
453 the Shelf region has a potential carbon uptake of 10.01±2.7 Tg C from February to early March,  
454 which accounts for approximately 5.0‰-6.7‰ of the net global ocean CO<sub>2</sub> uptake according to  
455 Takahashi et al. (2009), even though its total area is only 78\*10<sup>3</sup> km<sup>2</sup>. Due to the sill constraint,  
456 there is limited exchange between water masses in and outside the Prydz Bay. During winter, the  
457 dense water formed by the ejection of brine in the Bay can potentially uptake more  
458 anthropogenic CO<sub>2</sub> from the atmosphere that can descend to greater depths, thus enhancing the  
459 acidification in deep water. According to Shadwick et al. (2013), the winter values of pH and  $\Omega$   
460 decrease more remarkably than those in summer. As the bottom water in the Prydz Bay is a  
461 possible source of Antarctic Bottom Water (Yabuki et al., 2006), the Shelf region may transfer  
462 anthropogenic CO<sub>2</sub> at the surface to deep water and may thus influence the acidification of the  
463 deep ocean over long timescales.

464

#### 465 **4 Summary**

466 Based on the different observed ranges of the distribution of ocean pCO<sub>2</sub>, the Prydz Bay  
467 region was divided into three sectors from February to early March of 2015. In the Shelf region,  
468 biological factors exerted the main control on oceanic pCO<sub>2</sub>, while in the Open-ocean region,  
469 mixing and upwelling were the main controls. In the Sea-ice region, due to rapid changes in sea  
470 ice, oceanic pCO<sub>2</sub> was controlled by both biological and physical processes. SOM is an  
471 important tool for the quantitative assessment of oceanic pCO<sub>2</sub> and its subsequent sea-air carbon  
472 flux, especially in dynamic, high-latitude, and seasonally ice-covered regions. The estimated

473 results revealed that the SOM technique could be used to reconstruct the variations in oceanic  
474  $p\text{CO}_2$  associated with biogeochemical processes expressed by the variability in four proxy  
475 parameters: SST, CHL, MLD and SSS. The RMSE of the SOM-derived oceanic  $p\text{CO}_2$  is 22.14  
476  $\mu\text{atm}$  for the SOCAT dataset. From February to early March of 2015, the Prydz Bay region was a  
477 strong carbon sink, with a carbon uptake of  $23.57 \pm 6.36$  TgC. The strong potential uptake of  
478 anthropogenic  $\text{CO}_2$  in the Shelf region will enhance the acidification in the deep water region of  
479 the Prydz Bay and may thus influence the acidification of the deep ocean in the long run because  
480 it contributes to the formation of Antarctic Bottom Water.

#### 481 **Acknowledgments**

482 This work is supported by National Natural Science Foundation of China  
483 (NSFC41506209, 41630969, 41476172, 41230529), Qingdao National Laboratory for marine  
484 science and technology (QNL2016ORP0109), Chinese Projects for Investigations and  
485 Assessments of the Arctic and Antarctic (CHINARE2012-2020 for 01-04, 02-01, and 03-04).  
486 This work is also supported by Korea Polar Research Institute grants PE18060 and PE18070. We  
487 would like to thank China Scholarship Council (201704180019) and State Administration of  
488 Foreign Experts Affairs P. R. China for their support in this research. We would like to thank the  
489 carbon group led by Zhongyong Gao and Heng Sun in GCMAC and the crew on R/V Xuelong  
490 for their support on the cruise. We are thankful to contributors of the SOCAT database for  
491 validated  $p\text{CO}_2$  data and Mercator Ocean for providing the Global Forecast model output. We  
492 deeply appreciate Dr. Xianmin Hu in Bedford Institute of Oceanography, who provided us with  
493 useful technical instructions.

#### 494 **References**

- 495  
496 1. Bakker, D. C. E., Pfeil, B. Landa, C. S., Metzl, N., O'Brien, K. M., Olsen, A., Smith, K., Cosca,  
497 C., Harasawa, S., Jones, S. D., Nakaoka, S., Nojiri, Y., Schuster, U., Steinhoff, T., Sweeney,  
498 C., Takahashi, T., Tilbrook, B., Wada, C., Wanninkhof, R., Alin, S. R., Balestrini, C. F.,  
499 Barbero, L., Bates, N. R., Bianchi, A. A., Bonou, F., Boutin, J., Bozec, Y., Burger, E. F., Cai,  
500 W.-J., Castle, R. D., Chen, L., Chierici, M., Currie, K., Evans, W., Featherstone, C., Feely, R.  
501 A., Fransson, A., Goyet, C., Greenwood, N., Gregor, L., Hankin, S., Hardman-Mountford, N.  
502 J., Harlay, J., Hauck, J., Hoppema, M., Humphreys, M. P., Hunt, C. W., Huss, B., Ibáñez, J.  
503 S. P., Johannessen, T., Keeling, R., Kitidis, V., Körtzinger, A., Kozyr, A., Krasakopoulou, E.,

- 504 Kuwata, A., Landschützer, P., Lauvset, S. K., Lefèvre, N., Lo Monaco, C., Manke, A.,  
505 Mathis, J. T., Merlivat, L., Millero, F. J., Monteiro, P. M. S., Munro, D. R., Murata, A.,  
506 Newberger, T., Omar, A. M., Ono, T., Paterson, K., Pearce, D., Pierrot, D., Robbins, L. L.,  
507 Saito, S., Salisbury, J., Schlitzer, R., Schneider, B., Schweitzer, R., Sieger, R., Skjelvan, I.,  
508 Sullivan, K. F., Sutherland, S. C., Sutton, A. J., Tadokoro, K., Telszewski, M., Tuma, M., Van  
509 Heuven, S. M. A. C., Vandemark, D., Ward, B., Watson, A. J., and Xu, S.: A multi-decade  
510 record of high quality  $f\text{CO}_2$  data in version 3 of the Surface Ocean  $\text{CO}_2$  Atlas (SOCAT). *Earth  
511 System Science Data* 8: 383-413. doi:10.5194/essd-8-383-2016, 2016.
- 512 2. Barbini, R., Fantoni, R., Palucci, A., Colao, F., Sandrini, S., Ceradini, S., Tositti, L.,  
513 Tubertini, O., and Ferrari, G. M.: Simultaneous measurements of remote lidar chlorophyll  
514 and surface  $\text{CO}_2$  distributions in the Ross Sea. *International Journal of Remote Sensing*, 24,  
515 3807-3819, 2003.
- 516 3. Bates, N. R., Hansell, D. A., Carlson, C. A., and Gordon, L. I.: Distribution of  $\text{CO}_2$  species,  
517 estimates of net community production, and air-sea  $\text{CO}_2$  exchange in the Ross Sea polynya,  
518 *Journal of Geophysical Research*, 103, 2883-2896, 1998a.
- 519 4. Bates, N. R., Takahashi, T., Chipman, D. W., and Knapp, A. H.: Variability of  $p\text{CO}_2$  on diel  
520 to seasonal time scales in the Sargasso Sea, *Journal of Geophysical Research*, 103, 15567-  
521 15585, 1998b.
- 522 5. Brainerd, K. E., and Gregg, M. C.: Surface mixed and mixing layer depth, *Deep Sea Res., part  
523 A*, 42, 1521-1543, 1995.
- 524 6. Burkill, P. H., Edwards, E. S., and Sleight, M. A.: Microzooplankton and their role in  
525 controlling phytoplankton growth in the marginal ice zone of the Bellingshausen Sea, *Deep  
526 Sea Research Part II: Topical Studies in Oceanography*, 42(4), 1277-1290, 1995.
- 527 7. Chen, L., Xu, S., Gao, Z., Chen, H., Zhang, Y., Zhan, J., and Li, W.: Estimation of monthly  
528 air-sea  $\text{CO}_2$  flux in the southern Atlantic and Indian Ocean using in-situ and remotely sensed  
529 data, *Remote Sensing of Environment*, 115(8), 1935-1941, 2011.
- 530 8. Chierici, M., Olsen, A., Johannessen, T., Trinanes, J., and Wanninkhof, R.: Algorithms to  
531 estimate the carbon dioxide uptake in the northern North Atlantic using ship-observations,  
532 satellite and ocean analysis data, *Deep-Sea Res. Pt. II*, 56(8-10), 630-639, 2009.
- 533 9. Dandonneau, Y.: Sea-surface partial pressure of carbon dioxide in the eastern equatorial  
534 Pacific (August 1991 to October 1992): A multivariate analysis of physical and biological

- 535 factors, *Deep Sea Research II*, 42(2-3), 349-364, 1995.
- 536 10. Dong, S., Sprintall, J., Gille, S. T., and Talley, L.: Southern Ocean mixed-layer depth from  
537 Argo float profiles, *Journal of Geophysical Research*, 113, C06013, doi:  
538 10.1029/2006JC004051, 2008.
- 539 11. Edwards, A. M., Platt, T., and Sathyendranath, S.: The high-nutrient, low-chlorophyll regime  
540 of the ocean: limits on biomass and nitrate before and after iron enrichment, *Ecological*  
541 *Modelling*, 171, 103-125, 2004.
- 542 12. Friedrich, T., and Oschlies, A.: Basin-scale  $p\text{CO}_2$  maps estimated from ARGO float data: A  
543 model study, *J. Geophys. Res.*, 114, C10012, doi:10.1029/2009JC005322, 2009b.
- 544 13. Friedrich, T., and Oschlies, A.: Neural network-based estimates of North Atlantic surface  
545  $p\text{CO}_2$  from satellite data: A methodological study, *J. Geophys. Res.*, 114, C03020,  
546 doi:10.1029/2007JC004646, 2009a.
- 547 14. Gao, Z., Chen, L., and Gao, Y.: Air-sea carbon fluxes and there controlling factors in the  
548 PrydzBay in the Antarctic, *Acta OceanologicaSinica*, 3(27), 136-146, 2008.
- 549 15. Gibson, P. B., Perkins-Kirkpatrick, S. E., Uotila, P., Pepler, A. S., and Alexander, L. V.: On  
550 the use of self-organizing maps for studying climate extremes, *Journal of Geophysical*  
551 *Research: Atmospheres*, 122, 3891-3903, 2017.
- 552 16. Gibsonab, J. A.E., and Trullb, T. W.: Annual cycle of  $f\text{CO}_2$  under sea-ice and in open water  
553 in Prydz Bay, east Antarctica, *Marine Chemistry*, Volume 66, Issues 3-4, 187-200, 1999.
- 554 17. Hales, B., Strutton, P., Saraceno, M., Letelier, R., Takahashi, T., Feely, R., Sabine, C., and  
555 Chavez, F.: Satellite-based prediction of  $p\text{CO}_2$  in coastal waters of the eastern North Pacific,  
556 *Progress in Oceanography*, 103, 1-15, 2012.
- 557 18. Hardman-Mountford, N., Litt, E., Mangi, S., Dye, S., Schuster, U., Bakker, D., and Watson,  
558 A.: Ocean uptake of carbon dioxide ( $\text{CO}_2$ ), MCCIP BriefingNoteswww.mccip.org.uk, 9pp,  
559 2009.
- 560 19. Heil, P., Allison, I. and Lytle, V. I.: Seasonal and interannual variations of the oceanic heat  
561 flux under a landfast Antarctic sea ice cover, *J. Geophys. Res.*, 101(C11), 25,741-25,752, doi:  
562 10.1029/96JC01921, 1996.
- 563 20. Huang, J., Xu, F., Zhou, K., Xiu, P., and Lin, Y.: Temporal evolution of near-surface  
564 chlorophyll over cyclonic eddy lifecycles in the southeastern Pacific, *Journal of Geophysical*  
565 *Research: Oceans* 122, 6165-6179, 2017a.

- 566 21. Huang, W., Chen, R., Yang, Z., Wang, B., and Ma, W.: Exploring the combined effects of the  
567 Arctic Oscillation and ENSO on the wintertime climate over East Asia using self-organizing  
568 maps, *Journal of Geophysical Research: Atmospheres*, 122, 9107-9129, 2017b.
- 569 22. Iskandar, I.: Seasonal and interannual patterns of sea surface temperature in Banda Sea as  
570 revealed by self-organizing map, *Continental Shelf Research*, 30, 1136-1148, 2010.
- 571 23. Jacobs, S. S. and Georgi, D. T.: Observations on the south-west Indian/Antarctic Ocean, In *A*  
572 *Voyage of Discovery*, ed. by M. Angel, *Deep-Sea Res.*, 24(suppl.), 43-84, 1977.
- 573 24. Jamet, C., Moulin, C., and Lefèvre, N.: Estimation of the oceanic  $p\text{CO}_2$  in the North Atlantic  
574 from VOS lines in situ measurements: Parameters needed to generate seasonally mean maps,  
575 *Ann. Geophys.*, 25, 2247-2257, 2007, <http://www.ann-geophys.net/25/2247/2007/>.
- 576 25. Jiang, L. Q., Cai, W. J., Wanninkhof, R., Wang, Y., and Lüger, H.: Air-sea  $\text{CO}_2$  fluxes on the  
577 U.S. South Atlantic Bight: Spatial and seasonal variability, *Journal of Geophysical Research*,  
578 113 (2008), C07019, doi:10.1029/2007JC004366, 2008.
- 579 26. Jo, Y. H., Dai, M. H., Zhai, W. D., Yan, X. H., and Shang, S. L.: On the variations of sea  
580 surface  $p\text{CO}_2$  in the northern South China sea: A remote sensing based neural network  
581 approach, *Journal of Geophysical Research*, 117, C08022, doi:10.1029/2011JC007745, 2012.
- 582 27. Kohonen, T.: *Self-Organization and Associative Memory*, Springer, Berlin, 1984.
- 583 28. Lafevre, N., Watson, A. J., and Watson, A. R.: A comparison of multiple regression and neural  
584 network techniques for mapping in situ  $p\text{CO}_2$  data, *Tellus B*, 57(5), 375-384, 2005.
- 585 29. Laruelle, G. G., Landschützer, P., Gruber, N., Tison, J. L., Delille, B., and Regnier, P.: Global  
586 high resolution monthly  $p\text{CO}_2$  climatology for the coastal ocean derived from neural network  
587 interpolation, *Biogeosciences*, 14, 4545-4561, 2017.
- 588 30. Lei, R., Li, Z., Cheng, B., Zhang, Z., and Heil, P.: Annual cycle of landfast sea ice in Prydz  
589 Bay, East Antarctica, *Journal of Geophysical Research Atmospheres*, 115(C2), C02006,  
590 doi:10.1029/2008JC005223, 2010.
- 591 31. Liu C., Wang Z., Cheng C., Xia R., Li B., and Xie Z.: Modeling modified circumpolar deep  
592 water intrusions onto the Prydz Bay continental shelf, East Antarctica, *Journal of Geophysical*  
593 *Research*, Vol. 122, Issue 7, 5198-5217. DOI: 10.1002/2016JC012336, 2017.
- 594 32. Liu, Y., Weisberg, R. H., and He, R.: Sea Surface Temperature Patterns on the West Florida  
595 Shelf Using Growing Hierarchical Self-Organizing Maps, *Journal of Atmospheric and*  
596 *Oceanic Technology*, 23, 325-338, 2006.

- 597 33. Liu, Z. L., Ning, X. R., Cai, Y. M., Liu, C. G., and Zhu, G. H.: Primary productivity  
598 and chlorophyll a in the surface water on the route encircling the Antarctica during  
599 summer of 1999/2000, *Polar Research*, 112(4), 235-244, 2000.
- 600 34. Liu, Z., and Cheng Z.: The distribution feature of size-fractionated chlorophyll a and primary  
601 productivity in Prydz Bay and its north sea area during the austral summer, *Chinese Journal*  
602 *of Polar Science*, 14(2): 81-89, 2003.
- 603 35. Lüger, H., Wallace, D. W. R., Körtzinger, A., and Nojiri, Y.: The  $p\text{CO}_2$  variability in the  
604 midlatitude North Atlantic Ocean during a full annual cycle, *Global Biogeochem. Cycles*, 18,  
605 GB3023, doi:10.1029/2003GB002200, 2004.
- 606 36. Metzl, N., Brunet, C., Jabaud-Jan, A., Poisson, A., and Schauer, B.: Summer and winter air-sea  
607  $\text{CO}_2$  fluxes in the Southern Ocean, *Deep-Sea Research*, I53: 1548-1563, 2006.
- 608 37. Middleton, J. H., and Humphries, S. E.: Thermohaline structure and mixing in the region of  
609 Prydz Bay, Antarctica, *Deep Sea Research Part A, Oceanographic Research Papers*, 36(8),  
610 1255-1266, 1989.
- 611 38. Morrison, J. M., Gaurin, S., Codispoti, L. A., Takahashi, T., Millero, F. J., Gardner, W. D.,  
612 and Richardson, M. J.: Seasonal evolution of hydrographic properties in the Antarctic  
613 circumpolar current at 170W during 1997-1998, *Deep-Sea Research*, I48: 3943-3972, 2001.
- 614 39. Nakaoka, S., Telszewski, M., Nojiri, Y., Yasunaka, S., Miyazaki, C., Mukai, H., and Usui, N.:  
615 Estimating temporal and spatial variation of ocean surface  $p\text{CO}_2$  in the North Pacific using a  
616 self-organizing map neural network technique, *Biogeosciences*, 10, 6093-6106, 2013.
- 617 40. Nunes Vaz, R. A., and Lennon, G. W.: Physical oceanography of the Prydz Bay region of  
618 Antarctic waters, *Deep Sea Research Part I: Oceanography Research Papers*, 43(5), 603-641,  
619 1996.
- 620 41. Olsen, A., Trinanes, J. A., and Wanninkhof, R.: Sea-air flux of  $\text{CO}_2$  in the Caribbean Sea  
621 estimated using in situ and remote sensing data, *Remote Sens. Environ.*, 89, 309-325, 2004.
- 622 42. Pfeil, B., Olsen, A., Bakker, D. C. E., Hankin, S., Koyuk, H., Kozyr, A., Malczyk, J., Manke,  
623 A., Metzl, N., Sabine, C. L., Akl, J., Alin, S. R., Bellerby, R. G. J., Borges, A., Boutin, J.,  
624 Brown, P. J., Cai, W.-J., Chavez, F. P., Chen, A., Cosca, C., Fassbender, A. J., Feely, R. A.,  
625 González-Dávila, M., Goyet, C., Hardman-Mountford, N., Heinze, C., Hood, M., Hoppema,  
626 M., Hunt, C. W., Hydes, D., Ishii, M., Johannessen, T., Jones, S. D., Key, R. M., Körtzinger,  
627 A., Landschützer, P., Lauvset, S. K., Lefèvre, N., Lenton, A., Lourantou, A., Merlivat, L.,

- 628 idorikawa, T., Mintrop, L., Miyazaki, C., Murata, A., Nakadate, A., Nakano, Y., Nakaoka, Y.  
629 Nojiri, A. M. Omar, X. A. Padin, G.-H. Park, K. Paterson, F. F. Perez, S., Pierrot, D., Poisson,  
630 A., Ríos, A. F., Salisbury, J., Santana-Casiano, J. M., Sarma, V. V. S. S., Schlitzer, R.,  
631 Schneider, B., Schuster, U., Sieger, R., Skjelvan, I., Steinhoff, T., Suzuki, T., Takahashi, T.,  
632 Tedesco, K., Telszewski, M., Thomas, H., Tilbrook, B., Tjiputra, J., Vandemark, D., Veness,  
633 T., Wanninkhof, R., Watson, A. J., Weiss, R., Wong, C. S., and Yoshikawa-Inoue, H.: A  
634 uniform, quality controlled Surface Ocean CO<sub>2</sub> Atlas (SOCAT), *Earth Syst. Sci. Data*, 5, 125-  
635 143, doi:10.5194/essd-5-125-2013, 2013.
- 636 43. Pierrot, D., Neill, C., Sullivan, L., Castle, R., Wanninkhof, R., Lüger, H., Johannessen, T.,  
637 Olsen, A., Feely, R. A., and Cosca, C. E.: Recommendations for autonomous underway *p*CO<sub>2</sub>  
638 measuring systems and data-reduction routines, *Deep-Sea Research Part II*, 56, 512-522, 2009.
- 639 44. Rangama, Y., Boutin, J., Etcheto, J., Merlivat, L., Takahashi, T., Delille, B., Frankignoulle,  
640 M., and Bakker, D. C. E.: Variability of the net air-sea CO<sub>2</sub> flux inferred from shipboard and  
641 satellite measurements in the Southern Ocean south of Tasmania and New Zealand, *Journal*  
642 *of Geophysical Research: Oceans* (1978-2012), 110(C9), doi: 10.1029/2004JC002619, 2005.
- 643 45. Roden, N. P., Shadwick, E. H., Tilbrook, B., and Trull, T. W.: Annual cycle of carbonate  
644 chemistry and decadal change in coastal Prydz Bay, East Antarctica, *Marine Chemistry*,  
645 155(4), 135-147, 2013.
- 646 46. Rubin, S.I., Takahashi, T., and Goddard, J.G.: Primary productivity and nutrient utilization  
647 ratios in the Pacific sector of the Southern Ocean based on seasonal changes in seawater  
648 chemistry, *Deep-Sea Research I* 45, 1211-1234, 1998.
- 649 47. Sabine, L., Feely, R. A., Gruber, N., Key, R. M., Lee, K., Bullister, J. L., Wanninkhof, R.,  
650 Wong, S., Wallace, D. W. R., Tilbrook, B., Millero, F. J., Peng, T.-H., Kozyr, A., Ono, T.,  
651 and Rios, A. F.: The oceanic sink for anthropogenic CO<sub>2</sub>, *Science*, 305, 367-371,  
652 doi:10.1126/science.1097403, 2004.
- 653 48. Sarma, V. V. S. S., Saino, T., Sasaoka, K., Nojiri, Y., Ono, T., Ishii, M., Inoue, H. Y., and  
654 Matsumoto, K.: Basin-scale *p*CO<sub>2</sub> distribution using satellite sea surface temperature, Chl a,  
655 and climatological salinity in the North Pacific in spring and summer, *Global Biogeochemical*  
656 *Cycles*, 20, GB3005, doi:10.1029/2005GB002594, 2006.
- 657 49. Shadwick, E. H., Trull, T. W., Thomas, H., and Gibson, J. A. E.: Vulnerability of polar oceans  
658 to anthropogenic acidification: comparison of Arctic and Antarctic seasonal cycles, *Scientific*



- 659 Reports, 3: 2339, doi: 10.1038/srep02339, 2013.
- 660 50. Silulwane, N. F., Richardson, A. J., Shillington, F. A., and Mitchell-Innes, B. A.: Identification  
661 and classification of vertical chlorophyll patterns in the Benguela upwelling system and  
662 Angola-Benguela front using an artificial neural network, *South African Journal of Marine  
663 Science*, 23, 37-51, 2001.
- 664 51. Smith, N. R., Zhaoqian, D., Kerry, K. R., and Wright, S.: Water masses and circulation in the  
665 region of Prydz Bay Antarctica, *Deep-sea-research*, 31, 1121-1147, 1984.
- 666 52. Smith, N., and Tréguer, P.: *Physical and chemical oceanography in the vicinity of Prydz Bay,  
667 Antarctica*, Cambridge University Press, Cambridge, 1994.
- 668 53. Spreen, G., Kaleschke, L., and Heygster, G.: Sea ice remote sensing using AMSR-E 89 GHz  
669 channels, *J. Geophys. Res.*, 113, C02S03, doi:10.1029/2005JC003384, 2008.
- 670 54. Sun, W. P., Han, Z. B., Hu, C. Y., and Pan, J. M.: Particulate barium flux and its relationship  
671 with export production on the continental shelf of Prydz Bay, east Antarctica, *Marine  
672 Chemistry*, 157, 86-92, 2013.
- 673 55. Sweeney, C., Hansell, D. A., Carlson, C. A., Codispoti, L. A., Gordon, L. I., Marra, J., Millero,  
674 F. J., Smith, W. O., and Takahashi, T.: Biogeochemical regimes, net community production  
675 and carbon export in the Ross Sea, Antarctica, *Deep Sea Research II*, 47(15-16), 3369-3394,  
676 2000.
- 677 56. Sweeney, C.: The annual cycle of surface water CO<sub>2</sub> and O<sub>2</sub> in the Ross Sea: a model for gas  
678 exchange on the continental shelves of Antarctic, *Biogeochemistry of the Ross Sea, Antarctic  
679 Research Series*, 78, 295-312, 2002.
- 680 57. Sweeney, C.: The annual cycle of surface water CO<sub>2</sub> and O<sub>2</sub> in the Ross Sea: A model for gas  
681 exchange on the continental shelves of Antarctic, *Biogeochemistry of the Ross Sea, Antarctic  
682 Research Series*, 78, 295-312, 2002.
- 683 58. Takahashi, T. Feely, R. A., Weiss, R. F., Wanninkhof, R. H., Chipman, D. W., Sutherland,  
684 S. C., and Takahashi, T. T.: Global seaair CO<sub>2</sub> flux based on climatological surface ocean  
685 *p*CO<sub>2</sub>, and seasonal biological and temperature effects, *Deep-Sea Res. Pt. II*, 49(9-10), 1601-  
686 1622, 2002.
- 687 59. Takahashi, T., Sutherland, S. C., Wanninkhof, R., Sweeney, C., Feely, R. A., Chipman, D.  
688 W., Hales, B., Friederich, G., Chavez, F., Sabine, C., Watson, A. J., Bakker, D. C., Schuster,  
689 U., Metzl, N., Yoshikawa-Inoue, H., Ishii, M., Midorikawa, T., Nojiri, Y., Körtzinger, A.,

- 690 Steinhoff, T., Hoppema, M., Olafsson, J., Arnarson, T. S., Tilbrook, B., Johannessen, T.,  
691 Olsen, A., Bellerby, R., Wong, C. S., Delille, B., Bates, N. R., and de Baar, H. J. W.:  
692 Climatological mean and decadal change in surface ocean  $p\text{CO}_2$ , and net sea-air  $\text{CO}_2$  flux  
693 over the global oceans, *Deep-Sea Res. Pt. II*, 56(8-10), 554-577, 2009.
- 694 60. Takahashi, T., Sweeney, C., Hales, B., Chipman, D. W., Newberger, T., Goddard, J. G.,  
695 Iannuzzi, R. A., and Sutherland, S. C.: The changing carbon cycle in the Southern Ocean,  
696 *Oceanography*, 25, 26-37, 2012.
- 697 61. Telszewski, M., Chazottes, A., Schuster, U., Watson, A. J., Moulin, C., Bakker, D. C. E.,  
698 González-Dávila, M., Johannessen, T., Körtzinger, A., Lüger, H., Olsen, A., Omar, A., Padin,  
699 X. A., Ríos, A. F., Steinhoff, T., Santana-Casiano, M., Wallace, D. W. R., and Wanninkhof,  
700 R.: Estimating the monthly  $p\text{CO}_2$  distribution in the North Atlantic using a self-organizing  
701 neural network, *Biogeoscience*, 6, 1405-1421, 2009.
- 702 62. Thomson, R. E., and Fine, I. V.: Estimating mixed layer depth from oceanic profile data, *J.*  
703 *Atmos. Oceanic Technol.*, 20, 319-329, 2003.
- 704 63. Ultsch, A., and Röske, F.: Self-organizing feature maps predicting sea levels, *Information*  
705 *Sciences*, 144, 91-125, 2002.
- 706 64. Vesanto, J.: *Data Exploration Process Based on the Self-Organizing Map: the Finnish*  
707 *Academies of Technology*, 2002.
- 708 65. Wanninkhof, R.: Relationship between wind speed and gas exchange over the ocean revisited,  
709 *Limnology and Oceanography: Methods*, 12, 351-362, 2014.
- 710 66. Weiss, R. F.: Carbon dioxide in water and seawater: The solubility of a nonideal gas, *Marine*  
711 *Chemistry*, 2, 201-215, 1974.
- 712 67. Worby, A. P., Geiger, C. A., Paget, M. J., Van Woert, M. L., Ackley, S. F., and DeLiberty, T.  
713 L.: Thickness distribution of Antarctic sea ice, *Journal of Geophysical Research* 113, C05S92,  
714 <http://dx.doi.org/10.1029/2007JC004254>, 2008.
- 715 68. Wu, L., Wang, R., Xiao, W., Ge, S., Chen, Z., and Krijgsman, W.: Productivity-climate  
716 coupling recorded in Pleistocene sediments off Prydz Bay (East Antarctica), *Palaogeography,*  
717 *Palaeoclimatology, Palaeoecology*, 485, 260-270, 2017.
- 718 69. Xu, S., Chen, L., Chen, H., Li, J., Lin, W., and Qi, D.: Sea-air  $\text{CO}_2$  fluxes in the Southern  
719 Ocean for the late spring and early summer in 2009, *Remote Sensing of Environment*, 175,  
720 158-166, 2016.

- 721 70. Yabuki, T., Suga, T., Hanawa, K., Matsuoka, K., Kiwada, H., and Watanabe, T.: Possible  
722 source of the Antarctic Bottom Water in Prydz Bay region, *J. Oceanogr.*, 62, 649-655, doi:  
723 10.1007/s10872-006-0083-1, 2006.
- 724 71. Zeng, J. Nojiri, Y., Nakaoka, S., Nakajima, H., and Shirai, T.: Surface ocean CO<sub>2</sub> in 1990-  
725 2011 modelled using a feed-forward neural network, *Geoscience Data Journal*, 2, 47-51, doi:  
726 10.1002/gdj3.26, 2015.
- 727 72. Zeng, J., Mtsunaga, T., Saigusa, N., Shirai, T., Nakaoka, S., and Tan, Z.: Technical note:  
728 Evaluation of three machine learning models for surface ocean CO<sub>2</sub> mapping, *Ocean Sci.*, 13,  
729 303-313, <http://doi.org/10.5194/os-13-303-2017>, 2017.
- 730 73. Zeng, J., Nojiri, Y., Murphy, P. P., Wong, C. S., and Fujinuma, Y.: A comparison of  $\Delta p\text{CO}_2$   
731 distributions in the northern North Pacific using results from a commercial vessel in 1995-  
732 1999, *Deep Sea Res., Part II*, 49, 5303-5315, 2002.
- 733